JOURNAL of the MEXICAN CHEMICAL SOCIETY

https://www.jmcs.org.mx/

Article

Open Access

J. Mex. Chem. Soc. **2026**, *70(1):e2459*

Received March 13th, 2025
Accepted June 15th, 2025

http://dx.doi.org/10.29356/jmcs.v70i1.2459
e-location ID: 2459

Keywords:
Hydroxyapatite, SBS/hydroxyapatite composite, mechanical properties

Palabras clave:
Hidroxiapatita**,** material compuesto SBS/hidroxiapatita**,** propiedades mecánicas

***Corresponding author:**
Juventino López-Barroso
email: juventino.lb@queretaro.tecnm.mx
Phone: +52 9511998605

ISSN-e 2594-0317

Eggshell Waste Derived Hydroxyapatite-SBS Composites Toward a Sustainable Future in Polymer Recycling

Beatriz Adriana Salazar-Cruz[1], Cynthia Graciela Flores-Hernández[2], Alexia Guadalupe Dávila-Quiroz[1], José Luis Rivera-Armenta[1], Edgar Onofre-Bustamante[3], Juventino López-Barroso[2*]

[1]Centro de Investigación en Petroquímica, Tecnológico Nacional de México/ Instituto Tecnológico de Ciudad Madero, Pról. Bahía de Aldair y Ave. de las bahías, Parque de la pequeña y mediana industria, 89603, Altamira, Tamaulipas., México.
[2]División de Estudios de Posgrado e Investigación, Tecnológico Nacional de México/ Instituto Tecnológico de Querétaro, Av. Tecnológico S/n Esq. Gral. Mariano Escobedo, 76000, Querétaro, Querétaro, México.
[3]IPN, CICATA Unidad Altamira, Carretera Tampico-Puerto Industrial Altamira km 14.5, C. Manzano, Industrial Altamira, 89600 Altamira, Tamps.
Corresponding author: [2]; Avenida Tecnológico S/N, col Centro C. P. 76000.

Abstract. This research evaluated styrene-butadiene-styrene (SBS) composites modified with varying concentrations of hydroxyapatite (HAP) synthesized from eggshells. Hydroxyapatite is a versatile material with diverse applications, including its use as an adsorbent. The study investigated the incorporation of HAP particles into an SBS matrix a melt blending method in a mixing chamber. The composites were analyzed by X-ray diffraction (XRD), optical microscopy, infrared spectroscopy, and mechanical tests. The results indicate that incorporating hydroxyapatite significantly enhances several characteristics of the SBS composites, as evidenced by structural changes observed in XRD, morphological features revealed by optical microscopy, and improvements in mechanical strength and chemical properties according

J. Mex. Chem. Soc. **2026**, *70(1):e2459*
Regular Issue

ISSN-e 2594-0317

to the infrared analysis performed. The SBS/HAP composites containing synthetic hydroxyapatite derived from eggshells a 120 % improvement in mechanical properties compared to the reference sample, with compatibility between the components observed in the microscopy images.

Resumen. Esta investigación evaluó compuestos de estireno-butadieno-estireno (SBS) modificados con concentraciones variables de hidroxiapatita (HAP) sintetizada a partir de cáscaras de huevo. La hidroxiapatita es un material versátil con diversas aplicaciones, incluyendo su uso como adsorbente. El estudio investigó la incorporación de partículas de HAP en una matriz de SBS mediante un método de mezcla en fundido en una cámara de mezcla. Los compuestos se analizaron mediante difracción de rayos X (DRX), microscopía óptica, espectroscopia infrarroja y ensayos mecánicos. Los resultados indican que la incorporación de hidroxiapatita mejora significativamente varias características de los compuestos de SBS, como lo evidencian los cambios estructurales observados en la DRX, las características morfológicas reveladas por microscopía óptica y las mejoras en la resistencia mecánica y las propiedades químicas según el análisis infrarrojo realizado. Los compuestos de SBS/HAP que contienen hidroxiapatita sintética derivada de cáscaras de huevo mostraron una mejora del 120 % en las propiedades mecánicas en comparación con la muestra de referencia, con compatibilidad entre los componentes observada en las imágenes de microscopía.

Introduction

Hydroxyapatite (HAP) is a crystalline material primarily composed of phosphorus and calcium [1]. It is considered a biological material since it makes up approximately 65 % of the mineral fraction of bone [2,3]. While naturally occurring in the human body as a fundamental component of bone, HAP can also be synthesized artificially to produce synthetic HAP [4].

In recent years, green chemistry has focused on valorizing waste to reduce human impact on the environment. For example, some food residues have been used as precursors for novel materials, as reported by various authors [5-7].

Synthetic HAP serves as a bone substitute, composed of phosphate and calcium, with a structure similar to the inorganic component of human bone tissue. It is capable of biologically integrating into bone tissue without triggering an immune response, is not-toxic, and exhibits osteoconductive behavior [8-9].

Additionally, synthetic HAP demonstrates bioactivity, biocompatibility, and osteoconductivity, making it suitable for applications in bone repair, tissue engineering, drug and gene delivery, and other biomedical areas [10]. Moreover, due to its biological similarities to bone tissue and its relative abundance [11-13], HAP offers an eco-friendly solution in biomedical research and tissue engineering [4,14,15]. Animal-derived residues such as mammalian bones [16], fish spines and scales [17-19], and shells [20,21] play a significant role in the development of artificial substitutes for treating bone defects through the extraction of HAP.

One of the primary motivations for this research is the pressing issue of pollution. This study explores a potential alternative to repurpose waste, transforming it into a valuable material that positively impacts the environment and contributes to addressing national challenges. Utilizing waste in material production can significantly reduce the manufacturing costs of biomaterials while offering the added benefit of recycling, helping to mitigate waste pollution [6,22-23].

Several studies have proposed using eggshells as a calcium source in the preparation of HAP [24,25]. Eggshells are considered agro-industrial waste, and poor waste management leads to negative environmental impacts [26]. Chemically, eggshells are fundamentally composed of calcium carbonate (> 94 %) [3]. Multiple studies have explored their potential as a calcium precursor in the synthesis of HAP [27-29].

The use of HAP as a reinforcing material in polymeric composites has been explored to develop novel biomaterials, primarily focused on bone regeneration [30]. However, HAP is not limited to biomaterial applications; studies have investigated its use as an asphalt modifier [31], cure modifier [32,33], and flame retardant [33].

In these applications, the mechanical properties of rubber matrix have been scarcely studied. Specifically, understanding how HAP modifies the mechanical properties of styrene-butadiene-styrene (SBS) matrices remains as area of limited research. Addressing this knowledge gap could help establish the

J. Mex. Chem. Soc. **2026**, *70(1):e2459*
Regular Issue

ISSN-e 2594-0317

relationship between mechanical behavior and processing parameters. These findings could offer a new perspective on valorizing egg waste by transforming it into a functional reinforcing particle. Furthermore, these insights may lead to alternative studies on the effects of HAP particles on SBS properties.

This research focuses on obtaining HAP from biological waste, as reported elsewhere [27,28]. The goal of this study is to produce a composite using styrene-butadiene-styrene (SBS) thermoplastic elastomer and HAP at varying concentrations, utilizing the melting method in a mixing chamber. The mechanical, thermo-degradable, and morphological behavior of the resulting composite is evaluated.

Synthesizing SBS/HAP composites with HAP derived from eggshell waste is expected to improve mechanical properties, provided that compatibility between HAP and SBS is achieved.

Experimental

Materials

Ammonium phosphate ($NH_4H_2PO_4$, 98 % purity) and nitric acid (HNO_3, 70 % purity) were obtained from Fermont Company (Monterrey, Nuevo León, México). Radial-structure, thermoplastic copolymer styrene-butadiene-styrene blocks, containing 30 % total styrene, were donated by Dynasol Company (Altamira, Tamaulipas, México). Eggshell were sourced from food production waste.

Synthesis of hydroxyapatite from eggshell

Hydroxyapatite (HAP) was obtained from eggshells using the precipitation technique as the primary method of preparation [32]. Hen eggshells (*Gallus gallus*) were chosen as the substrate due to their high calcite content (95 % $CaCO_3$). The process began with the collection of eggshells from Distribuidora Allende (Tampico, Tamaulipas, México) followed by the removal of the inner membrane, yolk, and egg white. Only the shells were used. These were washed with water, dried at 60 °C for 24 hours, and then crushed until a particle size of 53 μm was achieved.

Chemical treatments

5% HNO_3 solution (Experiment 1)

A 1 L precipitated flask containing 74.8 mL of distilled water, 12 g of eggshell (53 μm), and 10 mL of a 4M $NH_4H_2PO_4$ solution was placed on a heating grill at 40 °C and stirred 150 rpm [34]. A 5 % HNO_3 solution was then added drop by drop. The addition of HNO_3 continued until effervescence, caused by the release of carbon dioxide as a reaction product, was no longer observed. The pH was monitored throughout and adjusted until reaching a final pH of 9.

HNO_3 solution (Experiment 2)

This synthesis was conducted following the method used in Experiment 1, with the variant being the concentration of the HNO_3 solution, which was set at 15 %. The reaction was considered complete when effervescence was no longer observed, after which the process continued until a final pH of 9 was reached.

Each experiment described above underwent a subsequent step in which the mixture was agitated for 4 h, then filtered and washed with distilled water to recover the precipitate generated in the chemical reactions described. The precipitate was then dried in an oven at 60 °C for 24 h (redLINE, Tuttlingen, Germany). Finally, the particle size of the sample was reduced using a porcelain mortar until a fine white powder was obtained.

Thermal treatment

For the heat treatment process to obtain HAP, the samples of Experiments 1 and 2 were placed in quartz canoes. These powdered materials were calcined in an TF55035A-1 furnace (Thermo Fisher Scientific, Asheville, NC, USA) using a temperature ramp as follows: from room temperature to 800 °C at a heating rate of 2 °C·min^{-1}. The samples were then maintained isothermally for 240 minutes, completing the sintering process before allowing the system to cool. The combination of chemical and thermal processes defines the synthesis of HAP [22].

http://dx.doi.org/10.29356/jmcs.v70i1.2459

J. Mex. Chem. Soc. **2026**, *70(1):e2459*
Regular Issue

ISSN-e 2594-0317

Obtaining SBS/HAP composites

To produce the SBS/HAP composites, the matrix was formed by adjusting the concentration of HAP across three distinct experiments while maintaining a consistent polymeric base. These experiments established three levels of HAP particle concentration in PHR (parts per hundred of rubber), as detailed in Table 1. These concentrations were applied for HAP obtained from 5 % and 15 % HNO_3 solutions.

The raw materials, consisting of the HAP and SBS mixture, were introduced into the mixing chamber under controlled temperature conditions. The composites underwent a melting process in a Brabender Intelli-Torque mixing chamber (Anton Paar, Duisburg, Germany) at 130 °C and 60 rpm for 15 minutes.

Subsequently, a compression process was used to form 2.5 mm composite films for characterization. The mold was rectangular, measuring 10 × 15 cm, with small composite pieces evenly distributed within it. Heating was conducted under pressure at 140 °C for 14 minutes. The pressure started at 0 bar for 5 minutes, gradually increasing to 100, 200, and 300 bar, with each increment maintained for 3 minutes, using a vertical hydraulic press (Dake, Shandong, China).

Finally, after cooling to 40 °C, uniformly thick composite plates were obtained for the creation of specimens for mechanical characterization tests [35].

Table 1. Experimental matrix for SBS/HAP composites.

Nomenclature	**Conditions of HAP obtention**	**Formulations**			
		100 SBS: 0 PHR	**100 SBS: 1 PHR**	**100 SBS: 5 PHR**	**100 SBS: 10 PHR**
		100	100	100	100
SBS	**No HAP added**	●			
5 % HNO_3 1 PHR	**HAP obtained in 5% HNO_3 solution**		●		
5 % HNO_3 5 PHR				●	
5 % HNO_3 10 PHR					●
15 % HNO_3 1 PHR	**HAP obtained in 15% HNO_3 solution**		●		
15 % HNO_3 5 PHR				●	
15 % HNO_3 10 PHR					●

Analysis

X-ray diffraction analysis

X-ray diffraction analysis provides detailed structural information, including chemical composition, crystallinity, crystal dimensions, deformations, and layer thickness. Characterization was performed using a D-5000 X-ray diffractometer (Siemens, Karlsruhe, Germany) equipped with an X-ray tube and cobalt anode (Co K_α 1.2 emission, $\lambda = 1.7903$ Å). The scanning range (2θ) was set from 0° to 70°, with a step size between 0.01° and 0.04° and counting time from 2 to 10 s.

Optical microscopy analysis

The investigation utilized an A1 Axio Lab optical microscope (Zeiss, Göttingen, Germany) equipped with 5×, 10×, and 40× magnification lenses, along with image processing software. This characterization technique was employed to analyze the dispersion morphology of the particles.

http://dx.doi.org/10.29356/jmcs.v70i1.2459

J. Mex. Chem. Soc. **2026**, *70(1):e2459*
Regular Issue

ISSN-e 2594-0317

Thermogravimetric analysis

The SBS/HAP compound (15 % HNO_3 solution with 10 PHR) obtained was analyzed using thermogravimetric analysis (TGA) with a simultaneous TGA/DSC analyzer (STD Q600, TA Instruments, New Castle, DE, USA). Reusable alumina sample holders containing 10 – 15 mg of sample were used in a controlled nitrogen (N_2) atmosphere at a flow of 100 mL min^{-1}. The analysis was conducted from room temperature up to 800 °C at a heating rate of 10 °C min^{-1}.

Tensile testing analysis

The test was conducted using a Model 5982 universal testing machine (Instron, Norwood, MA, USA) equipped with a 100 kN load cell. The six specimens analyzed for each test were in accordance with ASTM D412 [36].

Fourier Transform Infrared (FTIR) spectroscopy analysis

Fourier transform infrared (FTIR) spectroscopy was used to further confirm the chemical composition of the samples. The analysis was performed using a Fourier transform infrared spectrometer Spectrum One (Perkin Elmer, Frontier, Waltham, MA, USA) equipped with an Attenuated Total Reflectance (ATR) accessory. Sample preparation involved forming a film of SBS and composites, which were analyzed in the 400 – 4000 cm^{-1} range in transmission mode with a resolution of 4 cm^{-1}.

Results and discussion

X-ray diffraction analysis

The X-ray diffraction (XRD) technique is essential for identifying the characteristic elements present in the synthesis of HAP across the proposed experiments by generating diffraction patterns from the samples obtained in the different syntheses. Fig. 1 presents the diffraction pattern of the eggshell, labeled as "Eggshell" in this analysis. A distinct peak located at 2θ = 29.4°, corresponding to calcite – one of the primary components of eggshell – is clearly visible.

Additionally, Fig. 1 shows the results of experiments for HAP synthesis using 5 % and 15 % HNO_3 solutions. In these diffraction patterns, a series of characteristic peaks corresponding to the HAP structure are observed in the 2θ region at 25, 30, 32 33, 38, 40, 44, and 48 degrees. These results confirm the presence of HAP in both experiments.

It is noteworthy that these values are consistent with those obtained in previous studies [34]. using calcium and phosphorus precursor chemicals, where diffraction signals in the 2θ region at 25, 30, 32, 33, 40, 46, 48, and 50 degrees were also observed, further indicating the presence of HAP.

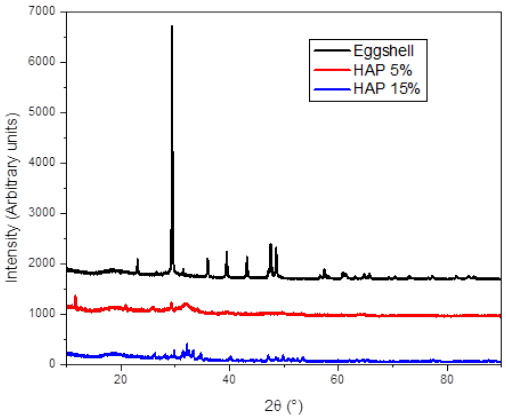

Fig. 1. Diffraction pattern of eggshell and HAP synthesized at 5 % and 15 % in HNO_3 solution.

http://dx.doi.org/10.29356/jmcs.v70i1.2459

J. Mex. Chem. Soc. **2026**, *70(1):e2459*
Regular Issue

ISSN-e 2594-0317

Optical microscopy

To investigate the interface of the SBS/HAP composites, optical microscopy analysis was conducted to evaluate the dispersion of HAP particles within the polymer matrix. Figures 2**(a-c)** show the SBS polymer without incorporating HAP particles, revealing inherent defects in the polymer. These surface irregularities may result from air retention during the pressing process, influenced by temperature and pressing time. Notably, the pressing methodology remained consistent across all evaluated composites.

Figures 2(d-f) present the SBS/HAP composite synthesized with a 5 % HNO_3 solution. The analysis reveals that the incorporated HAP particles tend to form heterogeneous agglomerations, which decrease as HAP concentration increases. Additionally, a porous morphology is observed, with the porosity increasing in tandem with concentration. This observation aligns with previous reports describing HAP as having a porous morphology with disordered crystalline aggregates. As the HAP concentration rises, the distribution shifts, reducing the separation between the agglomerates [8].

Figures 2**(g-i)** illustrate the SBS/HAP composite synthesized using a 15 % HNO_3 solution. A porous morphology is again observed, characterized by agglomerations of more uniform size but lacking a defined pattern. As concentration increases, the separation between agglomerates further decreases. Overall, HAP morphology appears irregular, with well-defined agglomerates and porous surfaces, consistent with other findings [37]. These observations provide valuable insights into the influence of HAP concentration on morphology and particle distribution within the SBS/HAP composite.

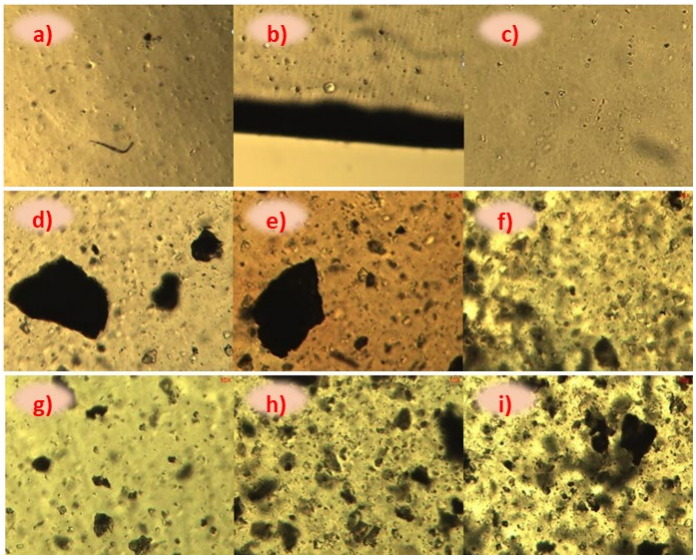

Fig. 2. In the upper line there are images from SBS at **(a)** 5x, **(b)** 10x, and **(c)** 40x lens. Then the middle line there are microscopies from SBS/HAP composites synthesized at 5 % HNO_3 at 10x with **(d)** 1 PHR, 5 PHR, and **(f)** 10 PHR. Finally, in the inferior line there are microscopy images from SBS/HAP composite synthesized at 15 % HNO_3, at 10x, **(g)** 1 PHR, **(h)** 5 PHR, **(i)** 10 PHR.

Thermogravimetric analysis (TGA)

TGA analysis allows for the observation of mass loss in the material as the temperature increases. Fig. 3 shows the relationship between material weight loss and temperature. Notably, the degradation and decomposition of the composites are very similar across all concentrations. Therefore, only a comparison between the SBS reference sample and the compound with the highest concentration – synthesized using a 15 % HNO_3 solution with 10 PHR – is presented.

Material loss began at 180 °C, aligning with previous findings [38]. It is important to note that the composite does not show significantly improved thermal degradation compared to the reference SBS. However, in the residue region, an increase in residue content is observed (from 1.18 % to 7.34 % for SBS and

J. Mex. Chem. Soc. **2026**, *70(1):e2459*
Regular Issue

ISSN-e 2594-0317

15%_HNO_3_10 PHR sample), primarily due to the presence of the inorganic HAP components, which remain stable and do not degrade within that temperature range, unlike the reference SBS.

The analysis in Fig. 3**(B)** presents the thermogram of the second derivative of weight for the composite at 10 PHR with synthesized HAP at 15 % HNO_3 compared to SBS. According to Fig. 3**(B)**, the onset of degradation begins at 330 °C for both SBS and the composite, followed by a maximum decomposition temperature at of 460 °C. This finding aligns with other studies [39], where the SBS polymer has been reported to begin decomposition at approximately 350 °C.

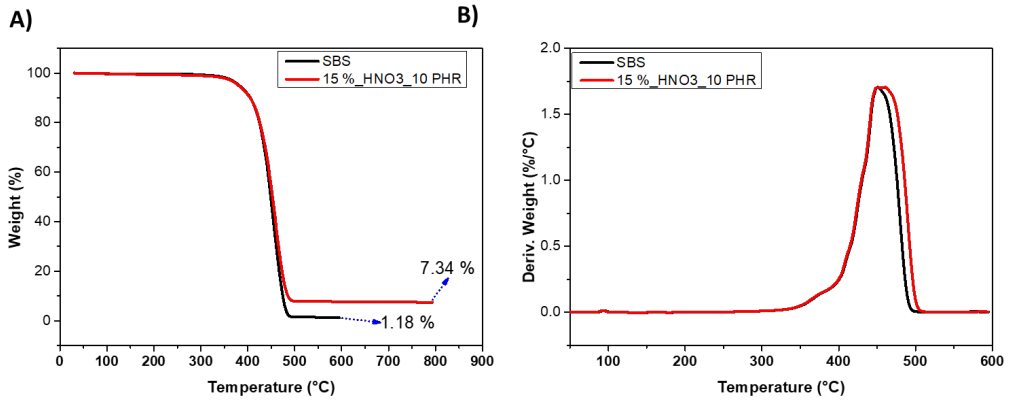

Fig. 3. (A) TGA thermogram of the SBS and the SBS/HAP composite at 10 PHR, synthesized HAP at 15 % HNO_3; **(B)** DTG of the of the SBS and the SBS/HAP composite at 10 PHR, synthesized HAP at 15 % HNO_3.

Tensile tests

Fig. 4 shows the stress-strain graph of the composites with two different HAP synthesis variants, as well as the reference sample. The composite with HAP synthesized using 15 % HNO_3 exhibits a higher stress at rupture – surpassing even the polymer without particles. The initial portion of the curve appears nearly linear, indicating that its slope represents the material's elastic modulus.

The addition of HAP influences both the tensile modulus and the material's flow characteristics. This effect has been previously reported [31,32], confirming that the incorporation of HAP improves the mechanical resistance. Principally, a homogeneous dispersion of HAP positively affects tensile properties [32,33]. In our case, the dual-extrusion mixer chamber facilitates the dispersion of HAP.

The change in modulus is attributed to van der Waals interactions between the HAP and SBS particles. According to Nihmath et al. [40], the compatibility of dipolar interaction groups in HAP with the rubber matrix enhances the reinforcement effect. Additionally, the inclusion of uniformly sized, smaller particles – observed in SEM images – leads to stronger HAP-SBS interactions. Consequently, the elastomeric matrix resists macromolecular chain deformations due to improved interfacial interactions.

Moreover, during the cooling process, the molten polymer contracts more rapidly than the HAP, generating compressive forces around the additive. The synthesis conditions of HAP further influence this effect. Tables 2 and 3 present the results for composites synthesized with 5 % and 15 % HNO_3, respectively. Specifically, when a 15 % HNO_3 solution is used in synthesis, the SBS exhibits a greater tendency for strain extension, as shown in Fig. 4**(b)**. The area under the tensile stress-strain curve, calculated from the average curve of each treatment, indicates increases of up to 80 % for the 15 % HNO_3 1 PHR composite.

Additionally, measurements such as maximum applied load, Young's modulus, yield load, and tensile deformation were obtained. The values from the analyzed samples reflect the statistical analysis of 6 repetitions, with standard deviations calculated for each series. The results are systematically tabulated and categorized according to property and concentration.

J. Mex. Chem. Soc. **2026**, *70(1):e2459*
Regular Issue

ISSN-e 2594-0317

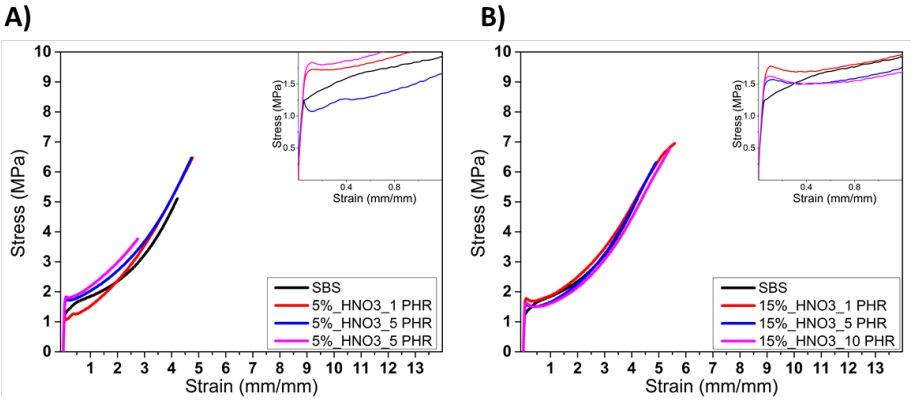

Fig. 4. Effect of HAP synthesis on tensile stress test of SBS/HAP composites with HAP synthesized with **(A)** 5 % of HNO_3 and **(B)** 15% HNO_3.

As shown in Tables 2 and 3, the composites synthesized with 15 % HNO_3 exhibit lower dispersion in their mechanical properties values. In contrast, the composites synthesized with 5 % HNO_3 show greater variations, particularly at low modifier concentrations (1 PHR). From these observations, it can be inferred that the composites containing HAP synthesized with 15 % HNO_3 demonstrate greater compatibility with the polymeric matrix, which aligns with the SEM images of SBS and the composites reported in this research.

Table 2. Mechanical tests for SBS/HAP composite with HAP synthesized with 5 % HNO_3 solution.

SBS/HAP composite with HAP synthesized with 5 % solution of HNO_3	Concentration (PHR)	Young´s modulus (MPa)	Maximum load (N)	Yield Load (At displacement 0.2 %, N)	Tensile strain at break (%)	Area under tensile-stress
	0	45.16 ±31.86	112.34 ±11.7	24.52 ± 2.7	517.03 ± 129.1	11.37
	1	49.12 ± 12.88	98.08 ±21.4	17.39 ± 1.7	535.12 ± 81.9	14.88
	5	24.74 ± 10.12	77.52 ±11.0	56.19 ± 2.5	577.91 ± 89.1	15.83
	10	47.19 ± 14.40	67.82 ± 9.42	20.74 ± 2.9	376.48 ± 61.31	6.94

Table 3. Mechanical tests for SBS/HAP composite with PAH synthesized with 15 % solution of HNO_3.

SBS/HAP composite with HAP synthesized with 15 % solution of HNO_3	Concentration (PHR)	Young´s modulus (MPa)	Maximum load (N)	Yield Load (At displacement 0.2 %, N)	Tensile strain at break (%)	Area under tensile-stress
	0	45.16 ± 31.86	112.34 ± 11.7	24.52 ± 2.7	517.03 ± 129.1	11.37
	1	31.14 ± 1.64	79.96 ± 16.8	34.56 ± 2.0	694.13 ± 10.3	20.54
	5	49.18 ± 11.05	83.33 ± 8.4	13.68 ± 4.3	630.2 ± 12.3	15.13
	10	34.99 ± 25.71	87.9 ± 5.6	33.18 ± 4.1	676.62 ± 26.5	17.55

http://dx.doi.org/10.29356/jmcs.v70i1.2459

J. Mex. Chem. Soc. **2026**, *70(1):e2459*
Regular Issue

ISSN-e 2594-0317

Analysis of variance

An analysis of variance (ANOVA) was conducted to evaluate the dispersion of HAP particles in the reference matrix across three concentrations (1, 5, and 10 PHR). Table 4 presents the ANOVA results for the composite synthesized with 5 % HNO_3, where concentration is the variable. The findings indicate that concentration significantly affects the composite's properties, consistently yielding higher values for the calculated critical factor compared to the predetermined critical factor.

Table 5 provides the results for the composite synthesized with 15 % HNO_3, showing that tensile deformation is the only property influenced by concentration. In contrast, the concentration of the PHR modifier does not impact the other properties.

Table 4. Results of ANOVA analysis composite SBS/HAP synthesized at 5 % HNO_3.

SBS/HAP with HAP synthesized with 5 % HNO_3 solution							
Model	**Sum of squares**	**D.F.**	**Average of squares**	**F calculated**	**Probability**	**Critical factor F**	**Influences**
Young's modulus	288639.17	2	144319.58	4.76	0.025	3.682	Yes
Load at yield	5406.88	2	2703.44	4.89	0.023	3.682	Yes
Deformation Tensile strain	140881.59	2	70440.79	6.45	0.009	3.682	Yes

Table 5. Results of ANOVA analysis composite SBS/HAP synthesized at 15 % HNO_3.

SBS/HAP with HAP synthesized with 5 % HNO_3 solution							
Model	**Sum of squares**	**D.F.**	**Average of squares**	**F calculated**	**Probability**	**Critical factor F**	**Influences**
Young's modulus	143180.76	2	71590.37	1.17	0.335	3.682	No
Load at yield	2214.85	2	1107.42	2.11	0.155	3.682	No
Deformation Tensile strain	93084.72	2	46542.36	11.09	0.001	3.682	Yes

Fourier transform infrared spectroscopy (FTIR)

Fig. 5**(A)** presents the IR spectra of SBS/HAP composites with varying HAP concentrations (1, 5, and 10 PHR), synthesized using a 5 % HNO_3 solution. The spectra were obtained using the film compression technique. The observed peaks highlight key features of polybutadiene units, with peaks at approximately 967, 745, and 911 cm^{-1}, corresponding to the stretching vibrations of (=C–H) trans bonds, (=C–H) cis bonds, and the vinyl group (= CH_2), respectively.

Additionally, the signal at 700 cm^{-1}, attributed to the poly(1-phenylethene-1,2-diyl) (polystyrene block), illustrates a distinctive feature of the SBS copolymer. This finding is consistent with Wang et al. [41], who identified these signals as characteristic of the SBS polymer, alongside a high Young's modulus value.

Several characteristic absorption bands corresponding to vibrational modes of the chemical bonds present in the sample are also evident. These absorption bands include: the 3570 cm^{-1} band, associated with the stretching vibration of the –OH groups in the hydroxyapatite structure; the 1090 cm^{-1} band, corresponding to

J. Mex. Chem. Soc. **2026**, *70(1):e2459*
Regular Issue

ISSN-e 2594-0317

the stretching vibration of phosphate (PO_4) bonds in HAP; and the 960 cm^{-1} band, related to the bending vibration of phosphate (PO_4) bonds in HAP.

Finally, a similar response was observed for composites synthesized with 15% of HNO_3, as evidenced in Fig. 5**(B)**.

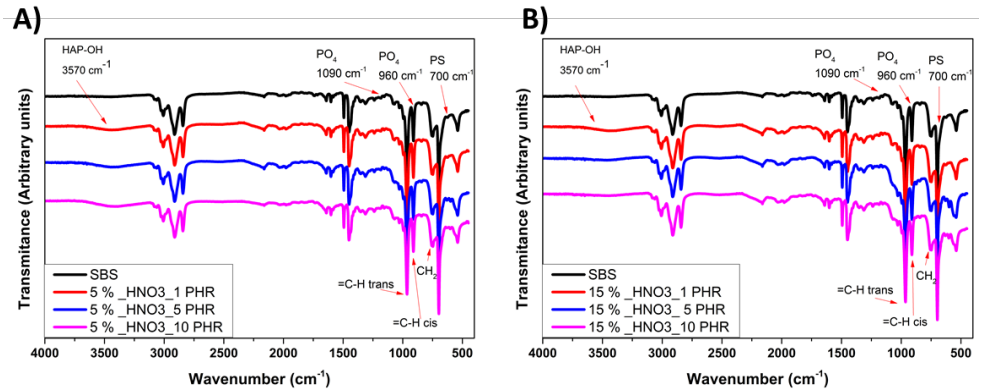

Fig. 5. IR spectra of SBS/HAP composites with HAP synthesized at A) 5% of HNO_3 and B) 15% HNO_3.

Conclusions

In this study, HAP was synthesized using the double decomposition method, and the influence of both the chemical treatment on HAP powder and the heat treatment was investigated using XRD, optical microscopy, and FTIR spectroscopy. Based on the results, it is concluded that synthesizing HAP from eggshells is feasible, as evidenced by various characterizations. XRD and FTIR confirm the presence of characteristic signals for apatite and demonstrate the influence of HAP on the matrix after its addition. This approach to valorizing eggshell waste also enabled the comparison of HAP synthesis using different solution methods.

Mechanical property results suggest a strong interaction in composites synthesized using the 15 % HNO_3 solution method. HAP particles synthesized with the 15 % HNO_3 solution show up to a 34 % increase in tensile strain at break (15 % HNO_3, 1 PHR) compared to the reference, indicating greater compatibility between the additive and the polymeric matrix. This is supported by the cooling behavior of the molten polymer, which contracts more significantly than the HAP composites.

Additionally, ANOVA reveals that variations in HAP synthesis have a significant effect on the composite properties, evidenced by the calculated critical factor consistently exceeding the reference critical factor. This difference suggests that modifications in HAP synthesis directly influence the final composite properties. Optical microscopy allowed an evaluation of HAP morphology within the composite and its compatibility with the polymer. The results indicate that the SBS/HAP composite synthesized with 5 % HNO_3 exhibits a more homogeneous particle distribution, with fewer agglomerations and a porous surface. Notably, both porosity and the homogeneity of the spaces between agglomerations increase as HAP concentration rises.

As future work, further more in-depth studies should be conducted on these materials. In particular, HAP derived from eggshells offers an eco-friendlier alternative for reinforcing rubber particles, as well as promise in environmental remediation applications.

References

1. Pramono, A.; Sulaiman, F.; Milandia, S.; Milandia, A. *IOP Conf. Ser.: Mater. Sci. Eng.* **2019**, *532*, 012004. DOI: https://doi.org/10.1088/1757-899X/532/1/012004

J. Mex. Chem. Soc. **2026**, *70(1):e2459*
Regular Issue

ISSN-e 2594-0317

2. Wibowo, C. H.; Ubaidillah, U.; Ariawan, D.; Surojo, E.; Nugroho, K. C.; Sunardi, S. *Discover Appl. Sci.* **2024**, *6*, 1–22. DOI: https://doi.org/10.1007/s42452-024-06098-4
3. Laohavisuti, N.; Boonchom, B.; Boonmee, W.; Chaiseeda, K.; Seesanong, S. *Sci. Rep.* **2021**, *11*, 15143. DOI: https://doi.org/10.1038/s41598-021-94643-1
4. Sadat-Shojai, M.; Khorasani, M. T.; Dinpanah-Khoshdargi, E.; Jamshidi, A. *Acta Biomater.* **2013**, *9*, 7591–7621. DOI: https://doi.org/10.1016/j.actbio.2013.04.012
5. Radha, K. V.; Selvi, V. S.; Aarcha, J. *Sustain. Chem. Clim. Action*. **2025**, *6*, 100056. DOI: https://doi.org/10.1016/j.scca.2025.100056
6. Khalid Zafeer, M.; Subrahmanya Bhat, K. *Sustain. Chem. Clim. Action.* **2023**, *2*, 100014. DOI: https://doi.org/10.1016/j.scca.2023.100014
7. Perera, U. P.; Foo, M. L.; Chew, I. M. L. *Sustain. Chem. Clim. Action.* **2023**, *2*, 100011. DOI: https://doi.org/10.1016/j.scca.2022.100011
8. Mondal, S.; Park, S.; Choi, J.; Vu, T. T. H.; Doan, V. H. M.; Vo, T. T.; Lee, B.; Oh, J. *Adv. Colloid Interface Sci.* **2023**, *321*, 103013. DOI: https://doi.org/10.1016/j.cis.2023.103013
9. Zaed, I.; Iaccarino, C.; Faedo, F.; Grillini, L.; Galassi, E.; Dotti, A.; Nataloni, A.; Mannella, F. C.; Cardia, A. *J. Appl. Biomater. Funct. Mater.* **2025**, 23. DOI: https://doi.org/10.1177/22808000241311389
10. Firdaus Hussin, M. S.; Abdullah, H. Z.; Idris, M. I.; Abdul Wahap, M. A. *Heliyon.* **2022**, *8*, e10356. DOI: https://doi.org/10.1016/j.heliyon.2022.e10356
11. Shi, H.; Zhou, Z.; Li, W.; Fan, Y.; Li, Z.; Wei, J. *Crystals*. **2021**, *11*, 149. DOI: https://doi.org/10.3390/cryst11020149
12. Murshed, M. *Cold Spring Harb. Perspect. Med.* **2018**, *8*, a031229. DOI: https://doi.org/10.1101/cshperspect.a031229
13. Pokhrel, S.; Pokhrel, S. *Adv. Chem. Eng. Sci.* **2018**, *8*, 225–240. DOI: https://doi.org/10.4236/aces.2018.84016
14. Hendi, A. A. *J. Alloys Compd.* **2017**, *712*, 147–151. DOI: https://doi.org/10.1016/j.jallcom.2017.04.021
15. Veluswamy, R.; Balasubramaniam, G.; Natarajan, M.; Krishnaswamy, M.; Chinnappan, B. A.; Nagarajan, S.; Subramanian, B.; Velauthapillai, D. *Sustain. Chem. Pharm.* **2024**, *41*, 101653. DOI: https://doi.org/10.1016/j.scp.2024.101653
16. Veremeev, A.; Bolgarin, R.; Nesterenko, V.; Andreev-Andrievskiy, A.; Kutikhin, A. *Materials.* **2020**, *13*, 3393. DOI: https://doi.org/10.3390/ma13153393
17. Mondal, B.; Mondal, S.; Mondal, A.; Mandal, N. *Mater. Charact.* **2016**, *121*, 112–124. DOI: https://doi.org/10.1016/j.matchar.2016.09.034
18. Gunduz, O.; Kilic, O.; Ekren, N.; Gokce, H.; Kalkandelen, C.; Oktar, F. N. *Key Eng. Mater.* **2017**, *720*, 207–209. DOI: https://doi.org/10.4028/www.scientific.net/KEM.720.207
19. Fara, A. N. K. A.; Abdullah, H. Z. *AIP Conf. Proc.* **2015**, 1669. DOI: https://doi.org/10.1063/1.4919215
20. El-Bassyouni, G. T.; Eldera, S. S.; Kenawy, S. H.; Hamzawy, E. M. A. *Heliyon.* **2020**, *6*, e04085. DOI: https://doi.org/10.1016/j.heliyon.2020.e04085
21. Suresh Kumar, C.; Dhanaraj, K.; Vimalathithan, R. M.; Ilaiyaraja, P.; Suresh, G. J. *Asian Ceram. Soc.* **2020**, *8*, 416–429. DOI: https://doi.org/10.1080/21870764.2020.1749373
22. Mohd Pu'ad, N. A. S.; Koshy, P.; Abdullah, H. Z.; Idris, M. I.; Lee, T. C. *Heliyon*. **2019**, *5*, e01588. DOI: https://doi.org/10.1016/j.heliyon.2019.e01588
23. Kardam, S.; Khanam, S. *Sustain. Chem. Clim. Action*. **2025**, *6*, 100055. DOI: https://doi.org/10.1016/j.scca.2024.100055

J. Mex. Chem. Soc. **2026**, *70(1):e2459*
Regular Issue

ISSN-e 2594-0317

24. Jaswal, A.; Samir, S.; Manna, A. *Trans. Indian Inst. Met.* **2023**, *76*, 2221–2230. DOI: https://doi.org/10.1007/s12666-023-02937-x
25. Wu, S.-C.; Hsu, H.-C.; Wang, H.-F.; Liou, S.-P.; Ho, W.-F. *Molecules*. **2023**, *28*, 4926. DOI: https://doi.org/10.3390/molecules28134926
26. Kareem, Z.; Eyiler, E. *RSC Adv.* **2024**, *14*, 21439–21452. DOI: https://doi.org/10.1039/d4ra02198c.
27. Haider, A.; Haider, S.; Han, S. S.; Kang, I. K. *RSC Adv.* **2017**, *7*, 7442–7458. DOI: https://doi.org/10.1039/c6ra26124h
28. Pandele, A. M.; Constantinescu, A.; Radu, I. C.; Miculescu, F.; Voicu, S. I.; Ciocan, L. T. *Materials.* **2020**, *13*, 274. DOI: https://doi.org/10.3390/ma13020274
29. Panda, M.; Joshi, S.; Annalakshmi, O.; Venkatraman, B. J. *Radioanal. Nucl. Chem.* **2024**, *334*, 807–816. DOI: https://doi.org/10.1007/s10967-024-09806-x
30. Ramesh, N.; Moratti, S. C.; Dias, G. J. *J. Biomed. Mater. Res., Part B.* **2018**, *106*, 2046–2057. DOI: https://doi.org/10.1002/jbm.b.33950
31. Li, J.; Wang, S.; Muhammad, Y.; Zhang, H.; Qiao, Q. *Constr. Build. Mater.* **2022**, *345*, 128361. DOI: https://doi.org/10.1016/j.conbuildmat.2022.128361
32. Hasan, L. A. *Saudi Dent. J.* **2021**, *33*, 1190–1196.DOI: https://doi.org/10.1016/j.sdentj.2021.01.001.
33. Maciejewska, M.; Rybiński, P.; Sowińska-Baranowska, A. *Materials*. **2024**, *17*, 3718. DOI: https://doi.org/10.3390/ma17153718
34. Oladipupo, O. F.; Adekola, A. H.; Ofudje, E. A.; Al-Ahmary, K. M.; Al-Mhyawi, S. R.; Alshdoukhi, I. F.; Alrahili, M. R.; Alsaiari, A. A. *Heliyon*. **2024**, *10*, e36493. DOI: https://doi.org/10.1016/j.heliyon.2024.e36493
35. Kribaa, O. K.; Latif, S.; Saifi, F.; Chahbaoui, N. *Mater. Today Proc.* **2022**, *49*, 1017–1022. DOI: https://doi.org/10.1016/j.matpr.2021.08.120
36. ASTM D412-16, Standard Test Methods for Vulcanized Rubber and Thermoplastic Elastomers—Tension; ASTM International: West Conshohocken, PA, 2021. DOI: https://doi.org/10.1520/D0412-16R21
37. Beh, C. Y.; Cheng, E. M.; Mohd Nasir, N. F.; Mohd Tarmizi, E. Z.; Eng, S. K.; Abdul Majid, M. S.; Ridzuan, M. J. M.; Khor, S. F.; Ahmad Saad, F. S. *J. Mater. Res. Technol.* **2020**, *9*, 14267–14282. DOI: https://doi.org/10.1016/j.jmrt.2020.10.012
38. Tukulula, M.; Hayeshi, R.; Fonteh, P.; Meyer, D.; Ndamase, A.; Madziva, M. T.; Khumalo, V.; Lubuschagne, P.; Naicker, B.; Swai, H.; Dube, A. *Pharm. Res.* **2015**, *32*, 2713–2726. DOI: https://doi.org/10.1007/s11095-015-1655-9
39. Thakur, V. K.; Grewell, D.; Thunga, M.; Kessler, M. R. *Macromol. Mater. Eng.* **2014**, *299*, 953–958. DOI: https://doi.org/10.1002/mame.201300368
40. Nihmath, A.; Ramesan, M. T. *Polym. Test.* **2020**, *91*, 106837. DOI: https://doi.org/10.1016/j.polymertesting.2020.106837
41. Liu, J.; Min, X.; Zhang, X.; Zhu, X.; Wang, Z.; Wang, T.; Fan, X. R. *Soc. Open Sci.* **2019**, *6*, 190536. DOI: https://doi.org/10.1098/rsos.190536